communications materials

A Nature Portfolio journal

Review article

https://doi.org/10.1038/s43246-025-00779-2

Advanced X-ray absorption spectroscopy for probing dynamics in CO_2 reduction reaction electrocatalysts

Beibei Sheng[1,2], Dengfeng Cao[1], Shuangming Chen[1] ✉, Nan Zhang[2], Jianqiang Wang[2] ✉ & Li Song[1] ✉

Electrochemical CO_2 conversion to value-added fuels presents an appealing avenue to realize low-carbon footprint. However, achieving sustainable energy conversion hinges on a comprehensive analysis of the catalyst surface-interface. X-ray Absorption Fine Structure (XAFS) spectroscopy emerges as a pivotal characterization technique to facilitate a profound comprehension of the structure-activity relationship at atomic and electronic scales. Particularly, it can serve as an efficient tool for in-situ monitoring of the dynamic evolution and surface-interface configuration of catalysts. Herein, we highlight the advantages of the traditional XAFS technique in probing charge transfer, electronic structure, valence state, geometric structure and local coordination environments, along with its application for discerning critical configurations and dynamic transformations of CO_2 reduction reaction (CO_2RR) electrocatalysts with high spatial-temporal resolution. Advanced XAFS techniques at next-generation synchrotron facilities hold great potential for unraveling the intricate processes and mechanisms of CO_2RR.

The rapid advancement of modern industrial society is intricately linked to various energy materials, notably fossil fuels. Currently, the utilization of fossil fuels has surged significantly, with demand continuing to rise[1,2]. This tendency not only contributes to energy depletion but also results in excessive CO_2 emissions, posing severe threats to the environment and human society[3]. In light of the global shift toward low-carbon energy, it is critical to mitigate the impact of CO_2 emissions and explore sustainable strategies to curtail CO_2 concentrations[4,5]. Among the multitude of approaches for CO_2 capture and utilization, electrochemical methods stand out for their ability to transform CO_2 into valuable chemical products or fuels[6,7]. These methods not only help reduce greenhouse gas emissions but also foster a circular carbon economy, thereby playing a critical role in combating climate change and promoting environmental sustainability[8,9].

In comparison to the electrocatalytic hydrogen evolution reaction (HER) and oxygen evolution reaction (OER), the carbon dioxide reduction reaction (CO_2RR) is notably more intricate, typically involving a multi-proton coupled electron process (PCET) at the interface of solid-liquid-gas[10]. Depending on the number of electrons transferred, a diverse array of products can be generated. Furthermore, addressing the selectivity issues stemming from various products and intermediates is crucial[11]. It is essential to accurately regulate these intermediates and reaction pathways, necessitating moderate binding energies of the intermediates at the active site[12,13]. Consequently, higher demands are placed on the understanding of the reaction mechanism and catalyst design, encompassing aspects like chemical composition, coordination environment, crystal structure, and dynamic changes. Achieving precise control over intermediates and reaction pathways is pivotal for advancing the efficiency and selectivity of CO_2RR processes[14,15].

To achieve this goal, it is essential to attain higher energy, temporal, and spatial resolutions at the molecular and atomic levels to uncover the structure and reaction mechanism of catalysts. While infrared spectroscopy (IR) can offer insights into the chemical properties of adsorbed species on electrocatalysts, the detection of the reaction process is often obscured by significant water molecule interference[16]. In contrast, Raman spectroscopy, characterized by a low scattering cross-section for water, can effectively provide distinctive structural information and insights into reaction intermediates under operational conditions[17]. However, this technique is less sensitive for metal-based electrocatalysts and reaction intermediates with low scattering cross-sections, rendering it primarily suitable for qualitative analyses[18]. Fortunately, X-ray absorption fine structure (XAFS) spectroscopy, leveraging synchrotron radiation light sources, can elucidate the local electronic structure and coordination environment of a specific element

[1]National Synchrotron Radiation Laboratory, Key Laboratory of Precision and Intelligent Chemistry, University of Science and Technology of China, Hefei, 230029, China. [2]SINOPEC Shanghai Research Institute of Petrochemical Technology Co. Ltd., Shanghai, 201208, China. ✉e-mail: csmp@ustc.edu.cn; wangjq.sshy@sinopec.com; song2012@ustc.edu.cn

within the catalyst[19,20]. Moreover, the development of advanced in-situ characterization methods enables the detection of the catalyst's dynamic structural evolution, and facilitates the monitoring of the catalyst structure and reaction mechanism simultaneously[21–23]. It can be argued that XAFS spectroscopy plays a pivotal role in every incremental advancement within CO_2 research. Thus, a comprehensive review is warranted to explore the latest developments in XAFS technology and its application in the realm of CO_2 research. Herein, we provide an in-depth exploration of characterization methods centered around XAFS, along with the advancements in emerging technologies like quick-scanning XAFS (QXAFS), high-energy-resolution fluorescence detected X-ray absorption spectroscopy (HERFD-XAS), difference XAFS (Δμ-XAFS), diffraction anomalous fine structure (DAFS), etc. developed in recent years for CO_2RR systems. We delve into the key factors influencing CO_2RR aiming to unveil the intricate structure and dynamic evolution of electrocatalysts at molecular, atomic, and electronic levels. Furthermore, we meticulously investigate the complexities and advancements in XAFS technology and CO_2RR systems, analyzing the challenges and opportunities they present. This discussion is conducive to offering insights that can guide the future development of catalysts and their practical industrial applications in the field of CO_2 reduction technologies.

Brief introduction of XAFS

The XAFS spectrum illustrates the relationship between the absorption coefficient (μ) of a particular element in a material and the energy (E) of incoming X-rays. Based on the formation mechanism and data processing approach, XAFS spectra can be categorized into two segments: the X-ray absorption near edge structure (XANES) spectrum (spanning from the pre-edge to 50 eV after the edge) and the extended X-ray absorption fine structure (EXAFS) spectrum (ranging from 50 to 1000 eV after the edge).

When incident X-ray photons possess energy equal to the ionization threshold of core-level electrons, these electrons undergo photoelectric absorption, resulting in the emission of photoelectrons. Consequently, a sharp discontinuity in the absorption coefficient occurs at this energy threshold, known as the absorption edge. The ejected low-energy photoelectrons experience multiple scattering events with neighboring coordinating atoms before returning to the absorbing atom, generating interference with the outgoing photoelectron wave and producing characteristic oscillations in the absorption spectrum. Conversely, when the incident energy is excessive, the photoelectron scatters from a single ligand atom near the absorbing atom and returns to interfere with the emitted wave, resulting in a less pronounced amplitude and a sinusoidal-like wave[24]. The XANES region conveys structural details such as valence state, d-band characteristics, charge transfer, orbital hybridization, symmetry, and the three-dimensional spatial arrangement of the specific absorbing atom. In contrast, the EXAFS portion offers insights into bond length, coordination number, and disorder factor of the nearest ligand atoms surrounding the specific absorbing atom.

In recent years, XAFS has witnessed a surge in its application within the catalysis field[25–27]. This technique is outstanding not only in meticulously examining minute alterations in bond lengths at the picometer scale resulting from surface relaxation and interactions with substrates, ligands, and adsorbates, but also in exploring the evolution of nanoscale morphology, macroscopic composition, and material structure. Moreover, XAFS can even generate heterogeneous distribution maps of various species within a macroscopic sample. This method plays a pivotal role in providing crucial insights into the identification of active species, their activation/inactivation processes, reaction intermediates, and underlying reaction mechanisms under *operando* conditions[28,29]. Figure 1 showcases the advancements and significant research discoveries stemming from the application of XAFS in CO_2RR recently. For instance, in 2020, Chen et al. introduced an *operando* X-ray absorption spectroscopy (XAS) approach using a quick-scanning monochromator to unveil the evolution of the metal chemical state in CO_2RR electrocatalysts with a time resolution in seconds[30]. In 2023, Yang et al. demonstrated the utility of *operando* HERFD-XAS for delving into critical surface chemistry insights during CO_2RR, boasting sub-electronvolt energy resolution[31]. Hwang et al. directly integrated MEA systems with *operando* XAS techniques to evaluate and analyze the eCO_2RR performance[32]. Given these advancements, our current focus revolves around the application of cutting-edge XAFS techniques from molecular, atomic, and electronic perspectives in the context of CO_2RR.

Application: XAFS probing local environment

X-ray absorption near edge structure. In the context of CO_2RR, the initial crucial step involves activating the CO_2 molecule[33]. As the CO_2 molecule attains dissolution equilibrium within the electrolyte, applying a voltage to facilitate electron transfer to CO_2 leads to the transformation of the CO_2 molecule into V-type $*CO_2^-$ on the surface of the electrode catalyst[34]. Subsequent PCET processes give rise to various C_1, C_2, C_3 intermediates, and end products[35,36]. Therefore, by fine-tuning the electronic structure of the catalyst and managing the charge transfer process, it is possible to establish active sites, optimize the adsorption energy of intermediates, and ultimately achieve heightened activity and selectivity in the reaction. As previously discussed, XANES is exceptionally sensitive to the state of unoccupied electrons[37]. Variations in oxidation state, electron structure, and charge transfer can be effectively discerned through shifts in the position of the pre-edge and the absorption edge. For instance, Liu et al. devised a Ni(I) monatomic catalytic active center with a d^9 electron configuration (A–Ni–NG and A–Ni–NSG). XANES described the delocalization of the unpaired electron within the Ni $3d_{x^2-y^2}$ orbital[38]. Notably, the edge peak intensity of Ni (II)Pc appeared faint, aligning with its elevated D_{4h} central symmetry. In the cases of A–Ni–NG and A–Ni–NSG, the heightened pre-edge peak intensity and the augmentation of dipole-allowed transitions ($1s \rightarrow 4p$) signify the emergence of a D_{4h} symmetrically distorted Ni(I) center, fostering enhanced adsorption of reactants and intermediates on the catalyst surface (Fig. 2a). Intriguingly, during the OCV state, the Ni K-edge energy within a CO_2-saturated $KHCO_3$ solution surpassed that in an Ar-saturated $KHCO_3$ solution by approximately 0.4 eV (Fig. 2b). This disparity arose from the intentional charge migration from Ni(I) to the C 2p orbital in CO_2, engendering a $CO_2^{\delta-}$ species, thereby diminishing the reaction's energy barrier (Fig. 2c). Furthermore, designing new catalysts based on the electronic structure of existing catalysts holds great importance in catalysis research. Through the utilization of *operando* Ni K-edge XANES spectra, Oh et al. successfully pinpointed the alterations in the electronic structure of NiS under the cathode potential of the CO_2RR[39]. The resulting $O_{x-z}S_y$ ligand exhibited analogous electronegativity and bond length to the N ligand in Ni–NC, consequently breaking the D_{4h} symmetry and leading to comparable electronic configurations (Fig. 2d, e). Moreover, XANES serves as a powerful tool in investigating charge transfer mechanisms between diverse components and elements within catalysts, encompassing alloy systems[40], interfacial charge transfer phenomena[41], and interactions between materials and substrates[42]. Such analyses bear significant implications for steering the development of catalysts characterized by high stability, activity, and selectivity under reduction conditions, thereby advancing the frontier of catalyst design for enhanced performance in various chemical processes.

During the actual reaction process, the application of a negative voltage triggers dynamic changes on the catalyst surface, leading to alterations in the valence state, atomic structure, and phase structure. Understanding the key factors that govern the CO_2RR and determining the true configuration of the catalyst during this dynamic process pose significant challenges. Linear combination fitting (LCF) proves invaluable for real-time monitoring of catalyst components under varying potential, facilitating the extraction of the dynamic chemical state of the active site during CO_2RR[43,44].

For p-zone metal oxides like SnO_2, preventing the formation of the metal phase at elevated reduction overpotentials is crucial for sustaining high stability. Oh et al. through in-situ XANES spectroscopy demonstrated that fluorine dopants play a pivotal role in preserving the elevated oxidation state and stability of tin[45] (Fig. 3a). Surfaces doped with fluorine in tin oxide

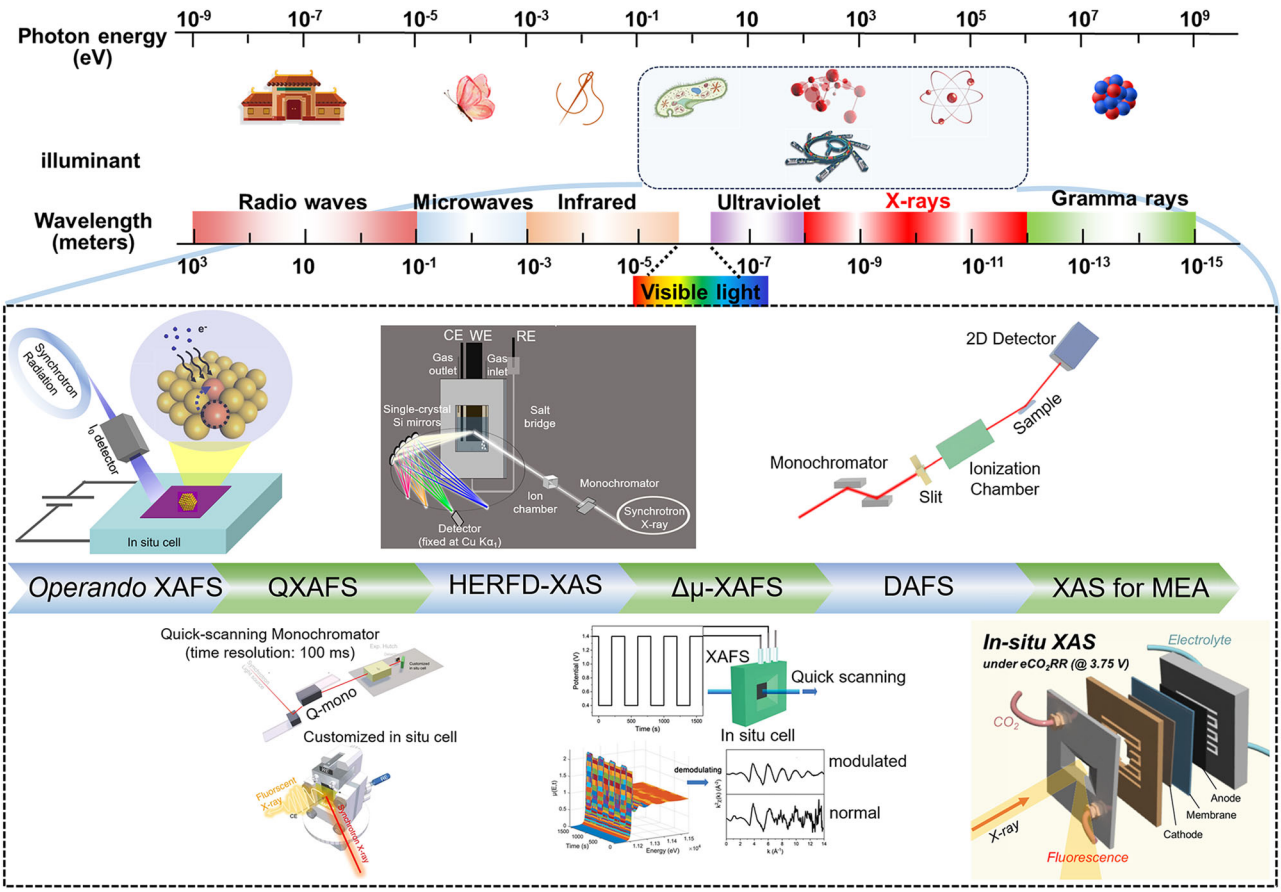

Fig. 1 | Summary of developed XAFS analytical techniques for CO_2RR. Nominal categorization of the distinct photon energy ranges that are accessible through synchrotron radiation, with the colored bands denoting the visible light spectrum. Advancements and significant research discoveries stemming from the application of XAFS in the realm of CO_2RR recently[30–32,41,80,98] (reproduced with permission from refs. 30–32,41,80,98. Copyright 2020, Springer Nature; Copyright 2023, American Chemical Society; Copyright 2023, American Chemical Society; Copyright 2022, International Union of Crystallography; Copyright 2020, American Chemical Society; Copyright 2024, The Royal Society of Chemistry).

(FTO) created a thermodynamically stable environment conducive to the formation of HCOO* intermediates compared to pure tin oxide surfaces. In the case of SnO_2 samples, notable changes in the absorption edge and white line peak were observed. Conversely, the spectrum of FTO exhibits only minimal energy shifts at the reduction potential, indicating minimal alterations in the oxidation state (Fig. 3b, c). LCF results offered an intuitive representation of this phenomenon, showcasing the preservation of the high oxidation state and stability of tin in FTO compared to pristine SnO_2 (Fig. 3d). Copper-based catalysts are widely employed, and the different valence states ($Cu^0/Cu^+/Cu^{2+}$) significantly influence product selectivity in catalytic reactions. For instance, Zheng et al. manipulated the structural reconstruction of $Cu_3(PO_4)_2$ under CO_2RR conditions with varying loads to selectively modulate product outcomes[46]. At lower loading capacities, the catalyst transitions to metallic Cu, favoring CO hydrogenation to CH_4. Conversely, higher $Cu_3(PO_4)_2$ loading foster a milieu where $Cu_3(PO_4)_2$ coexists with metallic Cu nanoparticles (Cu^0/Cu^{2+}), stimulating the dimerization of *CO to C_2H_4. Building upon this, Yang et al. screened $Cu_3(PO_4)_2$ derivative electrocatalysts based on copper phosphate, showcasing a stable Cu^0/Cu^{2+} interface through theoretical calculations[47]. In-situ X-ray XANES spectroscopy, aided by LCF, was employed on CuO and $Cu_3(PO_4)_2$ samples. Notably, Cu^{2+} exhibited a swifter conversion rate to Cu^0 compared to CuO. Following a 30-minute electrochemical reduction, nearly 73% of CuO samples were fully reduced to Cu^0, while 49% of $Cu_3(PO_4)_2$ samples retained Cu^{2+} states (Fig. 3e, f). *Operando* EXAFS analysis further substantiated these findings (Fig. 3g). The resultant Cu/CuPO catalyst yielded 69.7% FE for C_2H_4 and over 90% FE for C_{2+} in the effluent pool. At the stable Cu^0/Cu^{2+} interface, the Cu^{2+} site facilitated *CHO formation, which coupled with *CO on adjacent Cu^0 surfaces to generate *OCCHO, culminating in enhanced catalytic performance (Fig. 3h).

When the catalyst structure is unknown or significantly deviates from well-defined standard compounds, the utilizing of LCF can be challenging. In such cases, obtaining a detailed understanding of the complex geometric structure of the catalyst through XANES simulation becomes crucial. This approach helps establish the essential link between the catalyst's chemical state and the products[48,49]. For instance, Yao et al. leveraged *operando* XANES spectroscopy and XANES simulation to elucidate the surface reconstruction of CuAu–SAA under electrochemical conditions[50]. They observed the reversible migration of isolated Cu atoms from the vertex position of Au nanoparticles to the first atomic layer of Au, significantly modulating the electronic structure of Au and establishing it as the true active site (Fig. 4a, b). Cuenya et al. employed *operando* time-resolved XANES spectra to unveil local structures around Ni sites in transition metal nitrogen–carbon (TMNC) catalysts under actual operating conditions[51]. Initially, unsupervised machine learning methods like principal component analysis (PCA) combined with transformation matrix techniques were utilized to identify different coexisting nickel species, dynamic profiles, and XANES spectra (Fig. 4c, d). Subsequently, the atomic structure of each identified species was determined through an XANES simulation employing supervised machine learning techniques. Finally, the predicted structures' EXAFS spectra were validated using reverse Monte Carlo (RMC) simulations, enabling the identification of the initial TMNC catalyst structure, intermediate states, final structures, and the reconstruction of concentration distributions of various monatomic Ni species. These advanced methodologies offer powerful insights into the structural dynamics of

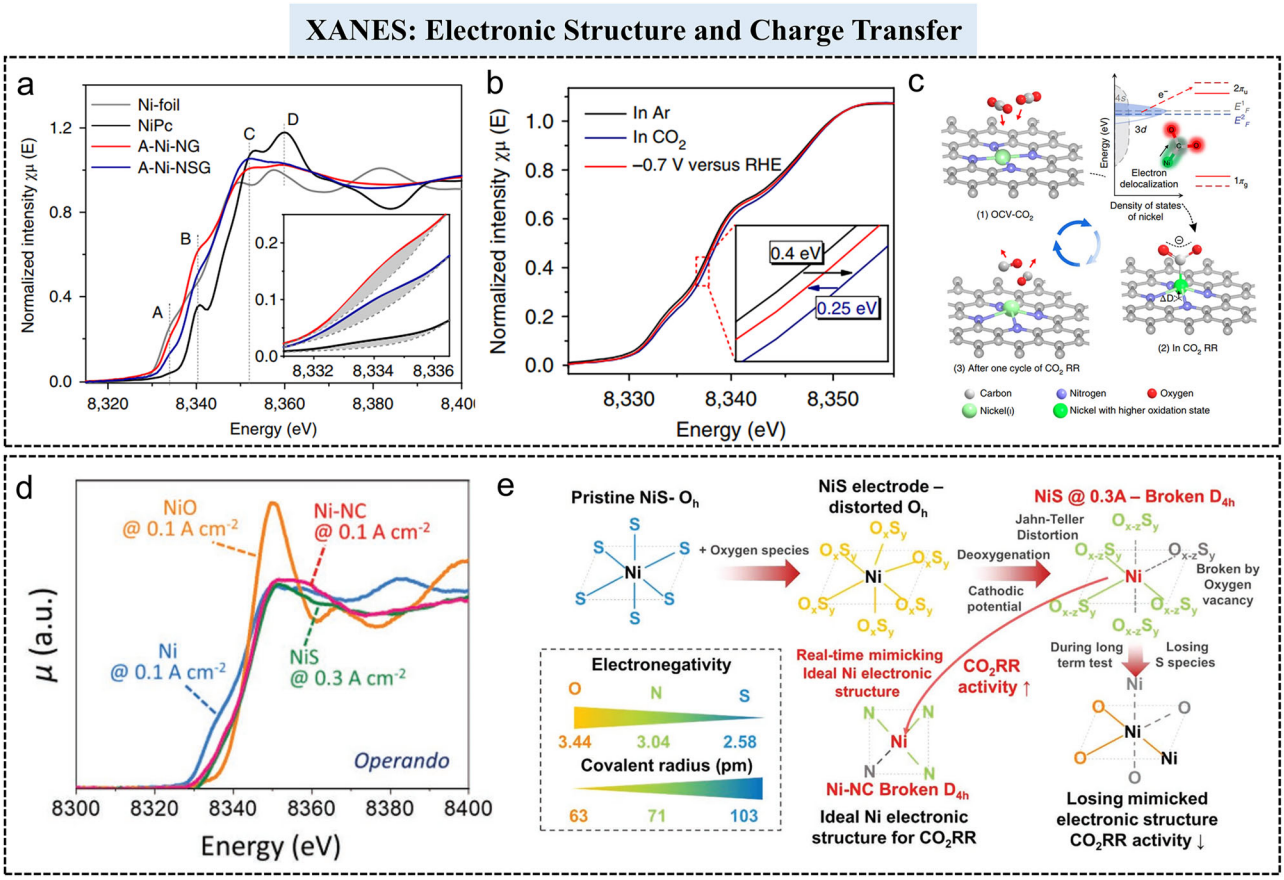

Fig. 2 | XANES spectra for electronic structure and charge transfer. a Ni K-edge XANES spectra of A–Ni–NG, A–Ni–NSG and NiPc. **b** Normalized *operando* Ni K-edge XANES spectra for A–Ni–NG at various biases in 0.5 M $KHCO_3$ aqueous solution at room temperature in 1 atm of Ar or CO_2. **c** Structural evolution of the active site in electrochemical CO_2 reduction[38] (**a**–**c** reproduced with permission from ref. 38. Copyright. 2018, Spring Nature). **d** Comparison of the various *operando* XANES spectra. **e** Schematic illustration of the expected origin of the electronic structure of NiS mimicking that of Ni–NC in real time[39] (**d**, **e** reproduced with permission from ref. 39. Copyright. 2022, Wiley-VCH GmbH).

catalysts under operational conditions, facilitating a deeper understanding of their behavior and catalytic mechanisms in complex reactions like CO_2RR.

Extended X-ray absorption fine structure. While XANES provides information about the electronic structure of materials, EXAFS complements this by offering insights into the local atomic arrangements and interactions, furnishing a more comprehensive understanding of the catalyst's properties. EXAFS analysis offers intricate details about the local atomic structure, with techniques like Fourier transform (FT) and wavelet transform (WT) enabling comprehensive analysis and visualization of EXAFS signals[52–54]. These methods facilitate the prompt identification of neighboring atoms, interatomic distances, coordination numbers, and can monitor the structure of single or diatomic atoms, interface bonding, catalyst structural changes, and other critical information. This detailed information, when analyzed concerning the electrocatalytic potential, aids in establishing the structure-activity relationship of catalysts in processes like CO_2RR. For instance, our research group utilized EXAFS to pinpoint CoNi two-site SACs for achieving high-yield syngas production[55]. Cao et al. devised a core-shell copper silicon catalyst (p-Cu@m-SiO_2) directly bonded via Cu–Si interactions, leading to a formation ratio of C_2H_4 to CH_4 spanning from 0.6 to 14.4[56]. Through the fitting of FT-EXAFS and WT-EXAFS, it was confirmed that the copper in p-Cu@mSiO_2 predominantly exists in a metallic Cu state. The absence of the Cu–O bond negates the presence of the Si–O–Cu structure at the Cu/SiO_2 interface, validating that the Cu (111) plane interacts with the SiO_2 shell through the Cu–Si bond (Fig. 5a–c). These findings underscore the significance of employing advanced techniques like EXAFS for unraveling intricate catalyst structures. Xia et al. have introduced a novel catalyst featuring a segregated Sb–Cu interfacial antimony copper single-atom alloy (Sb_1Cu) that displays remarkable efficiency in converting CO_2 to CO[57]. Analysis using FT-EXAFS revealed the absence of Sb–Sb bonds, indicating the presence of isolated Sb atoms. The identification of a Sb-Cu bond at a distance of 2.10 Å validates the successful formation of the Sb–Cu atomic interface, a critical aspect for the catalyst's performance. WT-EXAFS further corroborated this finding, solidifying the conclusion (Fig. 5d). In catalytic reactions, unsaturated sites are often recognized as highly active structures. Recently, our research group devised an Ni–N–C catalyst featuring unsaturated Ni sites coordinated with both pyridine and pyridine N in a dual coordination configuration (NiN_2)[58]. Notably, at a potential of −0.2 V_{RHE}, a peak position shift to approximately 1.47 Å was observed. Subsequently, as the potential dropped to −0.5 V_{RHE}, the formation of shorter Ni–C bonds resulted from CO adsorption, intensifying the leftward shift of the main peak. This peak intensity further increased as the potential decreased to −0.8 V_{RHE}, attributed to the accumulation of high concentrations of CO. The results from FT-EXAFS fitting demonstrated that the average coordination number of Ni increased by 0.25 at −0.5 V_{RHE} and by 0.36 at −0.8 V_{RHE} (Fig. 5e, f). This directly validates that the single CO adsorption Ni site within Ni−N−C serves as the primary active configuration, exhibiting high CO_2-to-CO catalytic activity (Fig. 5g).

The induction of unsaturated or low coordination sites through in-situ reconstruction of catalyst structures represent a potent strategy[59]. Cheng et al. conducted groundbreaking research on the dynamic

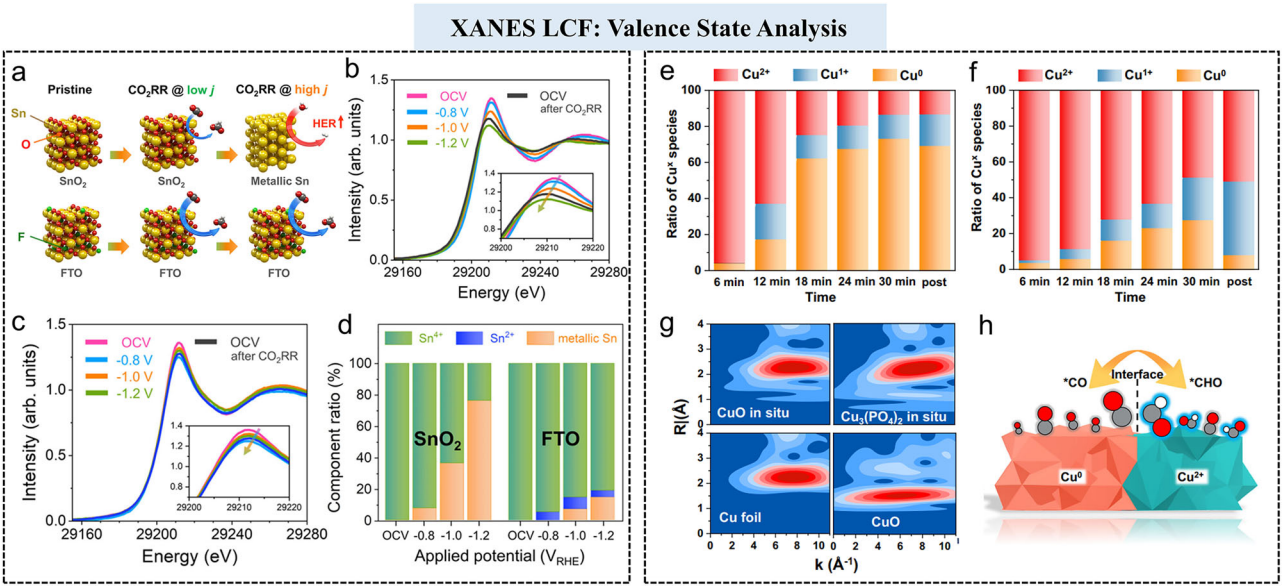

Fig. 3 | LCF for valence states analysis. a Schematic illustration of reaction affinity for SnO_2 and FTO under low/high cathodic overpotential. **b**, **c** *Operando* Sn K-edge XANES spectra for **b** SnO_2/C and **c** FTO/C catalysts during CO_2RR and **d** its oxidation state distribution deconvoluted by LCF (orange: Sn, blue: Sn^{2+}, and green: Sn^{4+})[47] (**a**–**d** reproduced with permission from ref. 47. Copyright 2023, Spring Nature). **e**, **f** Calculated ratio of Cu oxidation states in **e** CuO and **f** $Cu_3(PO_4)_2$ catalysts from LCF. **g** Morlet WT of the k^3-weighted *operando* EXAFS data for the $Cu_3(PO_4)_2$ and CuO samples with standard Cu foil and CuO powder as controls. **h** Schematic diagram of different intermediates on the Cu^0/Cu^{2+} interfaces[45] (**e**–**h** reproduced with permission from ref. 45. Copyright 2022, Spring Nature).

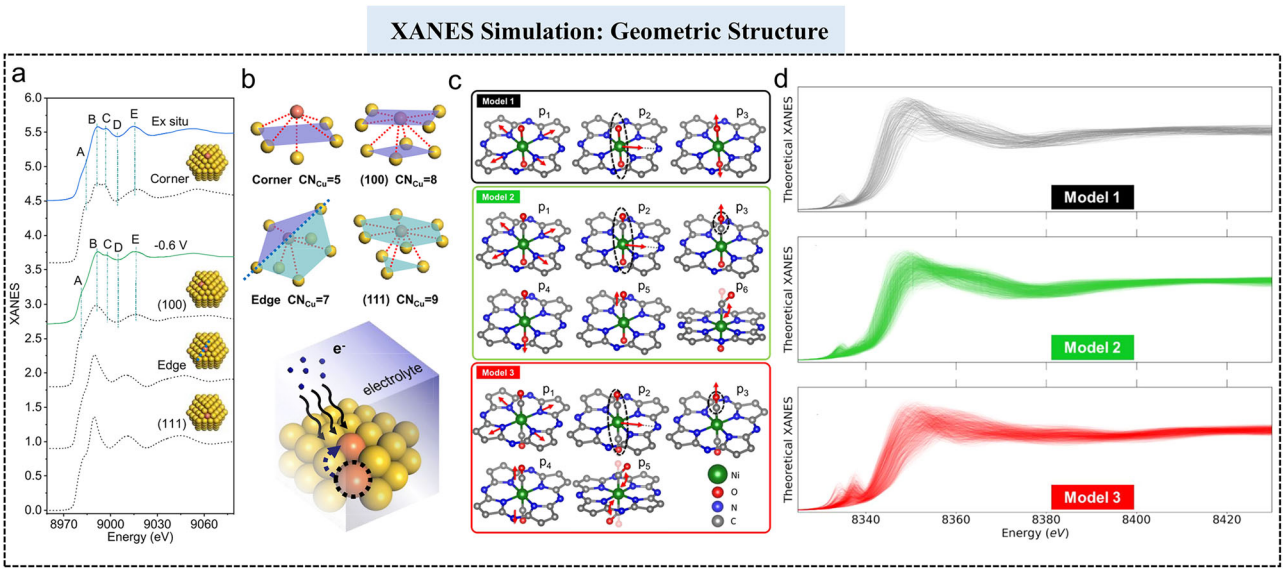

Fig. 4 | XANES Simulation for geometric structure analysis. a Cu K-edge XANES experimental spectra of the sample under ex situ condition and −0.6 V and the calculated spectra for Cu atoms at the corner, edge, (100) plane, and (111) plane and corresponding configurations. **b** Schematic for the coordination number of Cu atoms at different sites and the surface migration of single Cu atoms under working conditions[50] (**a**, **b** reproduced with permission from ref. 50. Copyright 2020, American Chemical Society). **c** Set of possible deformations applied to the structure models used for the construction of the SML training data set and XANES fitting. **d** Representative calculated XANES spectra for models 1–3[51] (**c**, **d** reproduced with permission from ref. 51. Copyright 2023, American Chemical Society).

reconstruction of atomically dispersed copper systems (N–Cu SAC) induced by potential, shedding light on the structure–activity relationship in CO_2RR[60]. *Operando* EXAFS spectroscopy unveiled the involvement of Cu–N bond breaking and Cu–Cu formation in the reconstruction of the N–Cu SAC, generating an adaptive low coordination configuration (Fig. 6a). Furthermore, in-situ experiments conducted at various potentials confirmed that this dynamic reconstruction is potential-dependent, irrespective of the electrolysis duration (Fig. 6b). This low coordination configuration, boasting an effective atomic surface charge, exhibits significantly heightened activity toward CO products compared to the conventional four-N coordination configuration. In recent developments, CO_2RR in acidic electrolytes has gained substantial attention due to its capability to effectively impede carbonate formation and enhance CO_2 utilization efficiency[61,62]. Xia et al. harnessed a catalyst derived from waste lead-acid batteries (Pb–$PbSO_4$) to efficiently and durably convert CO_2 into formic acid within a proton exchange membrane system[63]. Remarkably, they achieved a 91% single-pass CO_2 conversion efficiency and sustained operation for over 5200 h. In-situ EXAFS

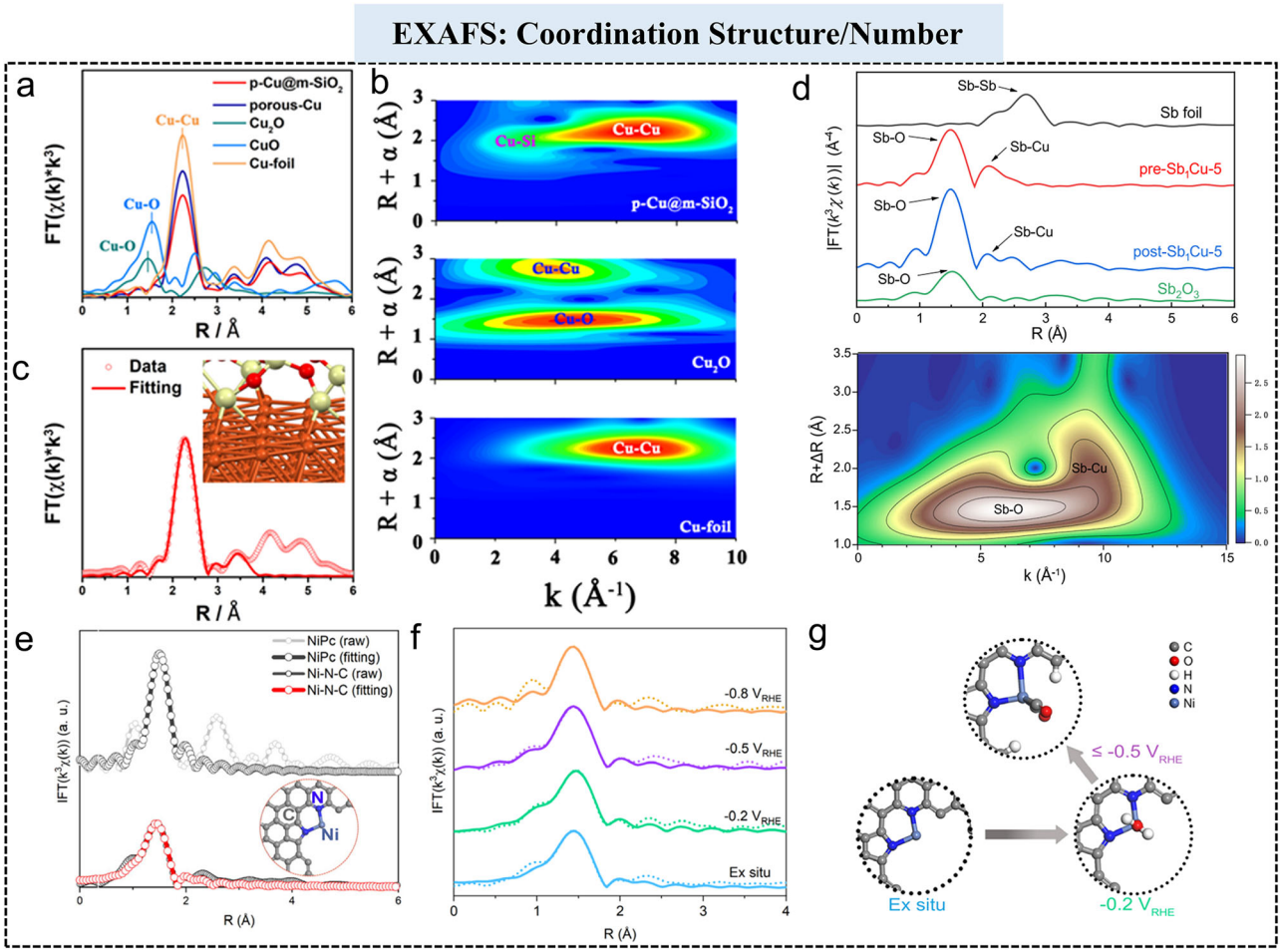

Fig. 5 | EXAFS for coordination structure and coordination number analysis. **a**, **b** Cu K-edge FT-EXAFS and WT-EXAFS spectra of p-Cu@m-SiO_2, porous-Cu, CuO, Cu_2O, and Cu-foil standard. **c** Fitting curves of FT-EXAFS spectra for p-Cu@m-SiO_2; Cu (orange), O (red), and Si (off-white)[56] (**a**–**c** reproduced with permission from ref. 56. Copyright 2024, American Chemical Society). **d** Ex situ FT-EXAFS and WT-EXAFS at the Sb K-edge of the as-prepared and post-catalysis Sb_1Cu-5[57] (**d** reproduced with permission from ref. 57. Copyright 2023, Spring Nature). **e** FT-EXAFS fitting results of Ni–N–C and NiPc. Inset shows the local coordination structure of Ni sites in Ni–N–C. **f** FT-EXAFS fitting results of Ni–N–C tested at various potentials. **g** Schematic illustration of the potential-induced structure changes of low-valence Ni sites in Ni–N–C[58] (**e**–**g** reproduced with permission from ref. 58. Copyright 2023, Spring Nature).

characterization captured the decline of the Pb-O/C peak and the rise of the Pb–Pb peak, indicating an increase in the proportion of metallic Pb. The observed redshift of the characteristic peak position around 2.2 Å signified the dynamic structural transformation from Pb–$PbSO_4$ to Pb–$PbCO_3$ (Fig. 6c). During the reaction process, the reduction of $PbCO_3$ was impeded, maintaining the stable Pb–$PbCO_3$ interface. Simultaneously, metallic Pb spontaneously converted to $PbCO_3$ with CO_2 and electrolyte flow. This dynamic Pb–$PbCO_3$ phase transition cycle generated active sites, ensuring the catalyst's high stability theoretically.

Emerging XAFS technology exploring structure–activity relationship

XAFS spectroscopy has been instrumental in elucidating the local and dynamic structural evolution of catalysts. While a typical XAFS spectrum acquisition process traditionally takes around a dozen minutes, this time-frame often insufficient to capture the rapid dynamics of electrocatalytic reactions that can occur within minutes. Recently, advancements in QXAFS technique were developed. Frahm and colleagues pioneered a revolutionary approach to X-ray absorption spectroscopy by introducing continuous oscillation of monochromator crystals (quick-scanning monochromator) to achieve rapid X-ray energy scanning through continuous Bragg angle adjustments[64]. This technique incorporated a high-speed data acquisition system that simultaneously records both the monochromator angle and X-ray intensity signals, departing from the traditional point-by-point scanning method of conventional XAFS. This innovation dramatically slashed acquisition times from seconds to milliseconds and has transformed QXAFS into a potent tool capable of real-time monitoring of kinetic processes, enabling the identification of intermediates and transient states in reactions[65–67]. This improved time resolution empowers researchers to delve deeper into the intricacies of catalytic mechanisms and transient species, shedding light on the dynamic nature of catalytic transformations with unprecedented detail and accuracy. For instance, Chen et al. pioneered the development of an effective in-situ TR-XAS technique to unveil the dynamic evolution of the near-surface chemical state of CuO_x under CO_2RR conditions[30]. When subjected to a using Redox Shuttle (R.S.) CuO_x exhibits a remarkable selectivity towards producing C_2H_5OH.The TR-XAS spectra captured at 5 s intervals depict a unique scenario where the chemical states of CuO_x oscillate between half Cu^0 and half Cu^+. Intriguingly, CuO_x treated using the conventional chronoamperometric methodology tended to transition into a predominantly Cu^0 state, thereby displaying heightened selectivity for CO production. This innovative approach provides valuable insights into the dynamic behavior of Cu-based catalysts and underscores the central role of in-situ techniques in unraveling the intricate mechanisms dictating catalytic selectivity and performance under *operando* conditions. Cuenya et al. conducted a groundbreaking study tracking the structural evolution of Cu–N–C catalysts utilizing QXAFS spectroscopy with a

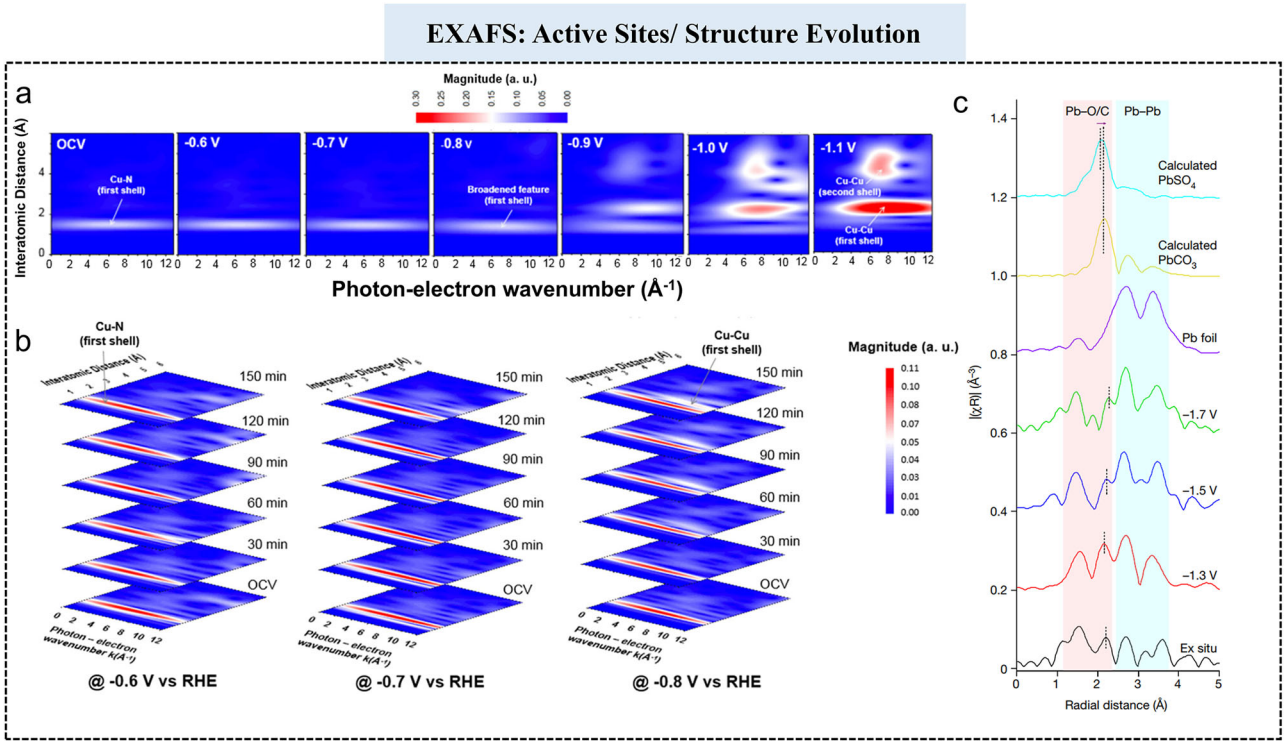

Fig. 6 | EXAFS for active sites and structure evolution analysis. a *Operando* Cu K-edge WT-EXAFS spectra of N–Cu SAC at various applied potentials. **b** *Operando* Cu K-edge WT-EXAFS spectra of N–Cu SAC at various applied potentials for 150 min[60] (**a**, **b** reproduced with permission from ref. 60. Copyright 2021, Spring Nature). **c** k^2-weighted Pb L_3-edge FT-EXAFS spectra along with the calculated $PbSO_4$ and $PbCO_3$ spectra as references[63] (**c** reproduced with permission from ref. 63. Copyright 2024, Spring Nature).

remarkable time resolution of up to 2 s per spectrum[68]. In a static CO_2RR scenario, Cu–SACs were observed to rapidly transition into Cu particles within a mere 100 s, with an average effective diameter of approximately 1.3 nm. During pulsed CO_2RR experiments, a series of intriguing periodic changes were noted: (i) a reduction in Cu–SAC sites, (ii) growth in the size of metallic Cu particles, (iii) fragmentation of Cu particles into smaller clusters, and (iv) subsequent transformation of these smaller Cu clusters back into Cu–SACs. By employing EXAFS fitting, the evolution of the CN of Cu–Cu over time was deduced, allowing for the estimation of nanoparticle sizes. The controlled modulation of these Cu species was found to be intricately linked to the selectivity observed in CO_2RR processes (Fig. 7). Specifically, Cu–SACs favored hydrogen production, ultra-small Cu clusters facilitated methane generation, while larger Cu nanoparticles predominantly produced CO and multi-carbon products.

Although synchrotron radiation light sources have seen rapid advancements in recent years, they still face limitations in providing sufficient energy resolution due to the inherent life broadening of the core hole, rather than being constrained by the resolution of the light source[69–71]. By employing a crystal Bragg optical analyzer in conjunction with a fixed-energy emission spectrometer, it becomes possible to enhance energy resolution[72]. This integration allows for the fluorescence yield to be concentrated over a narrow range centered on a specific fluorescence line, enabling the acquisition of high-resolution XAS spectra in a partial fluorescence yield (PFY) mode, as opposed to the total fluorescence yield (TFY). This technique, known as HERFD-XAS, offers an impressive energy resolution of 1 eV, surpassing traditional XAFS by 2-5 times[73] (Fig. 8a). In a study conducted by Yang et al., utilizing 5 nm Cu nanoparticles as the subject of investigation, the detection of Cu $K_{\alpha1}$ emission lines revealed that the overall energy resolution of *operando* HERFD-XAS stood at 0.66 eV, compared to the 1.6 eV resolution of traditional XAS methods[31]. Notably, an additional subtle pre-edge absorption feature observed at approximately 8977.2 eV, matching Cu–TDPA but not Cu_2O or CuO, indicated the presence of TDPA ligands on the surface of the original nanoparticles (Fig. 8b, c). This detail was indiscernible using traditional XAS techniques. The rapid decline in the intensity of the ligand peak under the applied potential, becoming invisible in the stable state, suggested complete detachment of the ligand from the Cu surface. Notably, low-coordination copper nanoparticles were identified as the actual active sites for the CO_2RR. Furthermore, their investigation extended to the I–AgCu electrocatalyst using *operando* HERFD-XAS[74]. The XANES spectra of the initial I–AgCu catalyst revealed the coexistence of metallic Cu and Cu_2O. As the reaction progressed, it was observed that metallic Cu transitioned into the active state for catalyzing CO_2RR within the AgCu system (Fig. 8d, e).

XAFS is a valuable technique for bulk characterization, but it encounters challenges when monitoring the subtle dynamic changes at the surface and interface where electrocatalytic reactions frequently occur. To address this limitation, a differential spectrum technique known as $\Delta\mu$-XAFS was developed. This method allows for the separation of the effects of adsorption reactants and active site evolution on the spectrum through direct differential procedures under varying potentials[62]. For instance, Jiang et al. introduced an in-situ HERFD-XANES method to unveil the dynamic structural evolution of the model catalyst CuPc in the CO_2RR[75]. By employing difference spectrum analysis and XANES simulations to eliminate information from atomically dispersed Cu species not involved in the reaction, they traced the transition from CuPc to Cu nanoparticles, shedding light on the process of Cu species aggregation. In another study, Cuenya et al. discussed the dynamic perturbation of a Cu_2O nanocube catalyst through pulse reactions[76]. By optimizing the dynamic equilibrium of copper surface species within a specific range of cathode and anode pulse durations, they achieved a twofold increase in ethanol production compared to static CO_2RR conditions. They observed that when the duration of the pulse was less than 1 s ($\Delta t_a < 1$ s), a distorted oxide structure might form on the surface, and the coexistence of metal and copper oxide species played a critical role in enhancing ethanol formation (Fig. 9a–d).

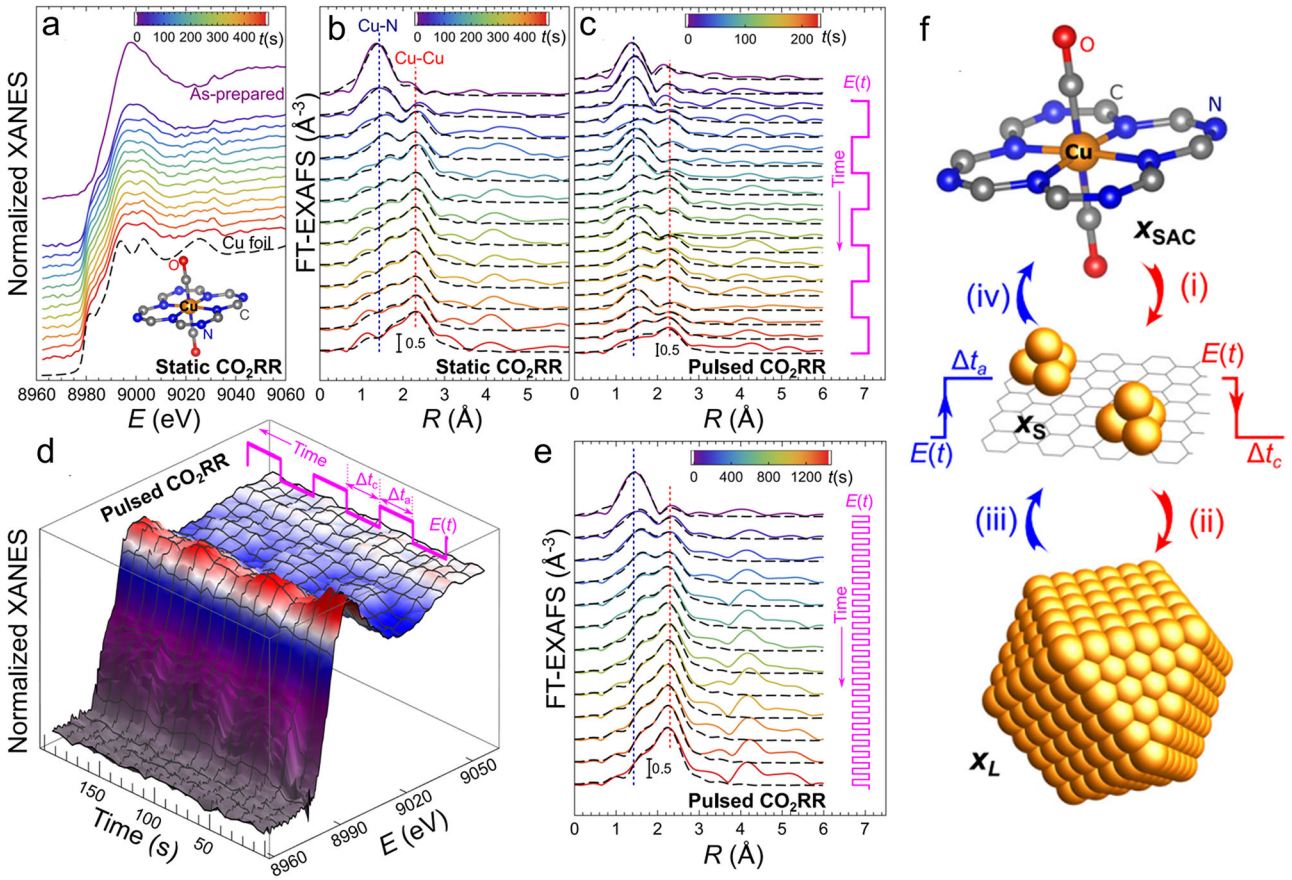

Fig. 7 | QXAFS technique exploring real-time kinetic processes. Cu K-edge XANES (**a**) and FT-EXAFS spectra (**b**) for Cu–N–C during the first 400 s of CO_2RR under static −1.35 V potential. The inset in **a** shows a structure model of the Cu single sites. Evolution of FT-EXAFS (**c, e**) and XANES (**d**) spectra during pulsed CO_2RR with $E_c = -1.35$ V, Ea = 0.44 V and $\Delta t_a = \Delta t_c = 30$ s. **c**, **d** Changes in the catalyst during the first 200 s under pulsed CO_2RR. **e** Changes in the catalyst during the first 1400 s under pulsed CO_2RR. Black dashed lines in (**b**, **c**, **e**)-EXAFS data fitting results. Vertical dotted lines in (**b**, **c**, **e**) mark the positions of the main FT-EXAFS features corresponding to the bonds between singly dispersed Cu sites and their nearest neighbors (blue line), and the Cu–Cu bonds in metallic Cu clusters (red line). Depicted spectra are averages over 20 s (**a**, **b**), 6 s (**c**, **d**) or 60 s (**e**). **f** Schematic representation of the main processes taking place under pulsed CO_2RR: conversion of singly dispersed sites into metallic species (i), particle growth (ii), fragmentation of particles (iii), and conversion of small clusters into singly dispersed sites (iv)[68] (reproduced with permission from ref. 68. Copyright 2024, Spring Nature).

Additionally, recent advancements in X-ray spectroscopy within the field of CO_2RR include the emergence of DAFS. DAFS spectroscopy is the oscillations in X-ray diffraction peak intensity near absorption edges, where the diffraction peak intensity is plotted against incident X-ray energy. The technique requires incident photon energies in proximity to the absorption edge of the element of interest. The unique advantage of DAFS lies in its ability to combine the long-range periodic order sensitivity of X-ray XRD with the local structural sensitivity of XAFS spectroscopy. This dual capability enables simultaneous characterization of long-range structure, local structure, and electronic structure[77–79]. A notable example is demonstrated in George et al.'s study of DAFS on Co_3O_4 (422) and (222) facets[78]. Since the measurements track diffraction peak intensity changes from these specific crystal planes, they selectively capture information about Co atoms residing in distinct crystallographic sites: the (422) plane exclusively contains Co atoms in tetrahedral coordination, while the (222) plane contains only octahedrally coordinated Co atoms. By extracting XAFS information from these DAFS measurements, researchers obtained site-specific absorption spectra distinguishing between octahedral and tetrahedral Co environments, effectively achieving site-selective XAFS analysis. Recently, our group have successfully extracted EXAFS data from the Cu (111) plane using electrochemically modulated differential spectra and DAFS spectra, elucidating the transition from a Cu_2O and Cu heterostructure to a stepped Cu site[80] (Fig. 9e, f). Despite its advantages, DAFS presents significant technical challenges. The technique imposes strict sample requirements: strong and well-defined X-ray diffraction peaks, compatibility with fluorescence XAFS measurements, presence of a center of symmetry, and sufficient radiation resistance etc. In contrast, traditional XAFS offers greater flexibility, capable of analyzing even amorphous materials. DAFS measurements demand sophisticated experimental configurations and prolonged data collection periods due to the necessity for precise angular alignment and energy scanning. The data analysis is particularly complex, requiring simultaneous consideration of both diffraction and absorption phenomena. While traditional XAFS lacks site selectivity, it offers broader sample compatibility and simpler experimental implementation. Given these considerations, researchers must develop proficiency in various advanced XAFS characterization techniques and carefully select appropriate methodologies based on their specific experimental systems and research objectives.

Conclusion and future outlook

As discussed in this review, electrochemical conversion CO_2 to valuable products offers a sustainable solution to achieve an artificially closed carbon cycle. However, the CO_2RR involving solid–liquid–gas three-phase interfaces is actually quite complex. Beyond catalysts and reaction processes, engineering aspects also play a crucial role in understanding this multifaceted process. To gain a profound insight into the CO_2RR, sophisticated characterization techniques are imperative. Among these techniques, XAFS stands out as a powerful approach, being capable of unveiling the elemental composition and clarifying the complex relationship between structure and performance at the electronic scale. In this review, the pivotal role of

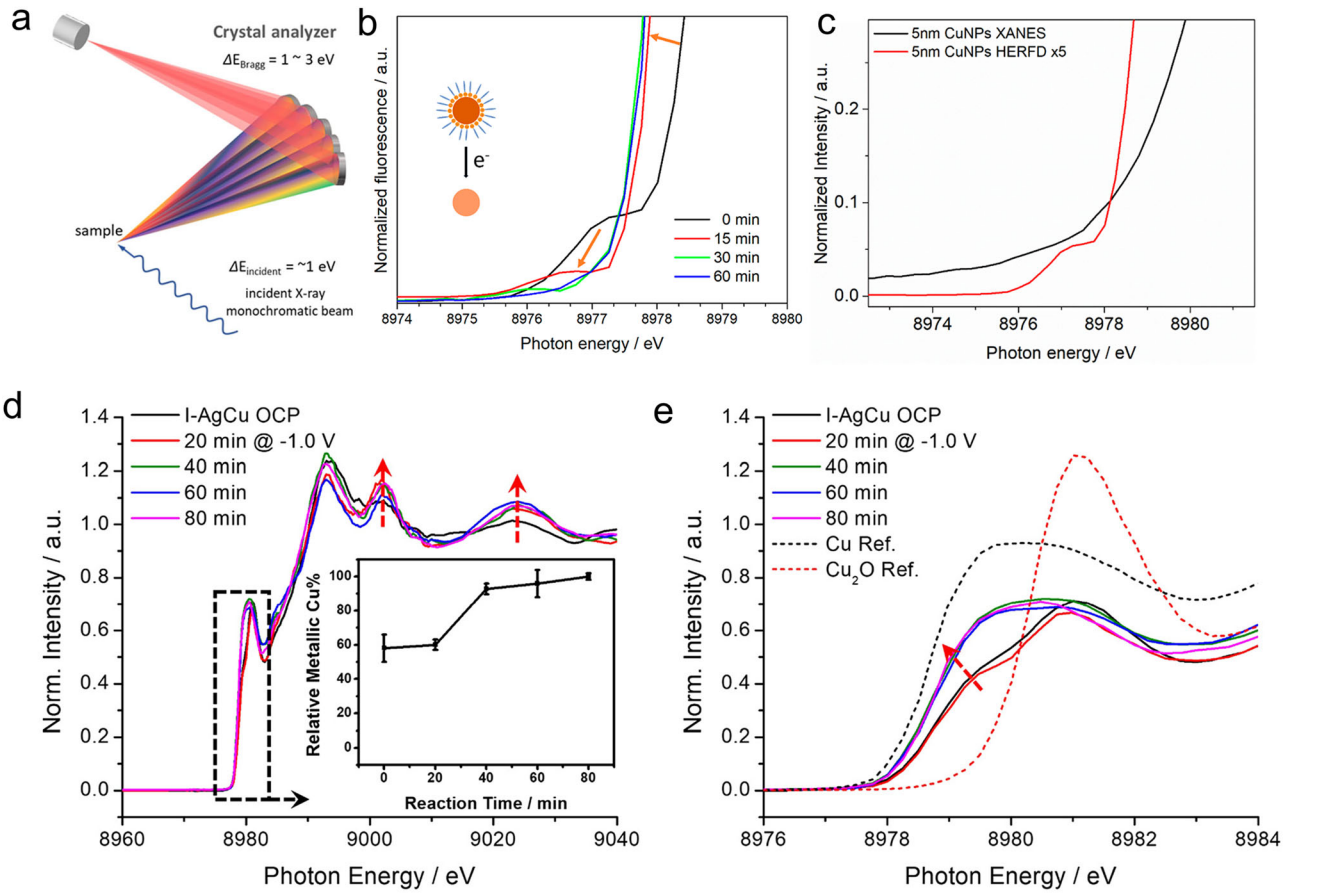

Fig. 8 | HERFD XANES exploring structure-activity relationship with high-resolution. a Schematic of fluorescence detection by Bragg crystal analyzer[73] (**a** reproduced with permission from ref. 73. Copyright 2023, Spring Nature). **b** *Operando* HERFD-XANES characterization for the magnification of the ligand feature near 8977.2 eV, showing its fast decrease and eventual disappearance. **c** Comparison of conventional and HERFD XANES of 5 nm Cu NPs at OCP[31]. (**b**, **c** reproduced with permission from ref. 31. Copyright 2023, American Chemical Society). **d** Operando HERFD XANES of Cu K-edge of the I–AgCu as a function of the reaction time at −1.0 V vs RHE in CO_2-saturated 0.1 M $KHCO_3$. The inset shows the quantitative analysis of the relative metallic Cu fraction. **e** XANES pre-edges of I–AgCu magnified from the dashed box region in (**d**) and the comparison with Cu and Cu_2O references (dashed lines)[74] (**d**, **e** reproduced with permission from ref. 74 Copyright 2023, American Chemical Society).

advanced XAFS techniques is discussed in exploring the evolution of composition, charge transfer, oxidation state, electronic structure, and local coordination environment of the catalyst throughout the adsorption, conversion, and desorption stages of the CO_2RR. Moreover, higher time resolution QXAFS captures the dynamic evolution of electrochemical processes at the scale of seconds or milliseconds, while high energy resolution HERFD-XAFS can identify buried finer configurations. $\Delta\mu$-XAFS shines brightly in identifying surface structural information and subtle changes in CO_2RR. DAFS can simultaneously acquire information on both long-range and short-range ordered structures. Despite the significant advancements achieved, there still remain many challenges in fully comprehending the dynamic nature of the reaction. Continued exploration and refinement of advanced XAFS methodologies are crucial for gaining a deeper understanding of the dynamic processes involved in electrochemical CO_2 conversion. For examples:

(1) Enhancing the extraction of high-quality XAFS signals at the surface interface influenced by low-concentration CO_2. In current laboratory CO_2RR, high-purity processed CO_2 is utilized instead of the low concentrations of CO_2 typically found in industrial flue gas, which often contains impurities like N_2, O_2, NO_x, and SO_x[81]. This not only elevates the raw material costs but also contaminates the catalyst's active sites. Consequently, the direct electric reduction of low-concentration CO_2 emerges as a more energy-efficient yet challenging strategy for resource utilization[82]. Currently, researchers are dedicated to using solid electrolytes or enhancing CO_2 enrichment through organic material modifications[83,84]. Moreover, the co-reduction of CO, CO_2, and N_2 to generate urea or ammonia presents an efficient avenue for CO_2 conversion[85–87]. However, the selection of appropriate gas component ratios and the optimization of organic matter and electrolyte selections continue to be focal points for researchers. Furthermore, assistance is required in the following areas.

(2) In-situ cell optimization and industrial catalysts design. The in-situ reaction cell or reactor assumes a crucial role in studying these reactions. Both the electrolytes and input/output gases present within the reactor can influence XAFS signals. Disturbances caused by these factors can significantly impact comprehension of real reaction processes. Hence, the optimization of in-situ cell design requires several critical considerations. Firstly, specialized flow channel systems, such as spiral or serpentine configurations, should be implemented to enhance fluid turbulence and optimize inlet and outlet positions, thereby eliminating dead zones. Secondly, careful material selection is essential: radiation-resistant cell materials (such as Teflon and polyether ether ketone) should be utilized, alongside appropriate window materials (including Kapton membranes, etc.). The electrode materials must balance corrosion resistance with electrical conductivity, while sealing materials should provide both excellent gas-tight properties and radiation resistance. Thirdly, dimensional parameters

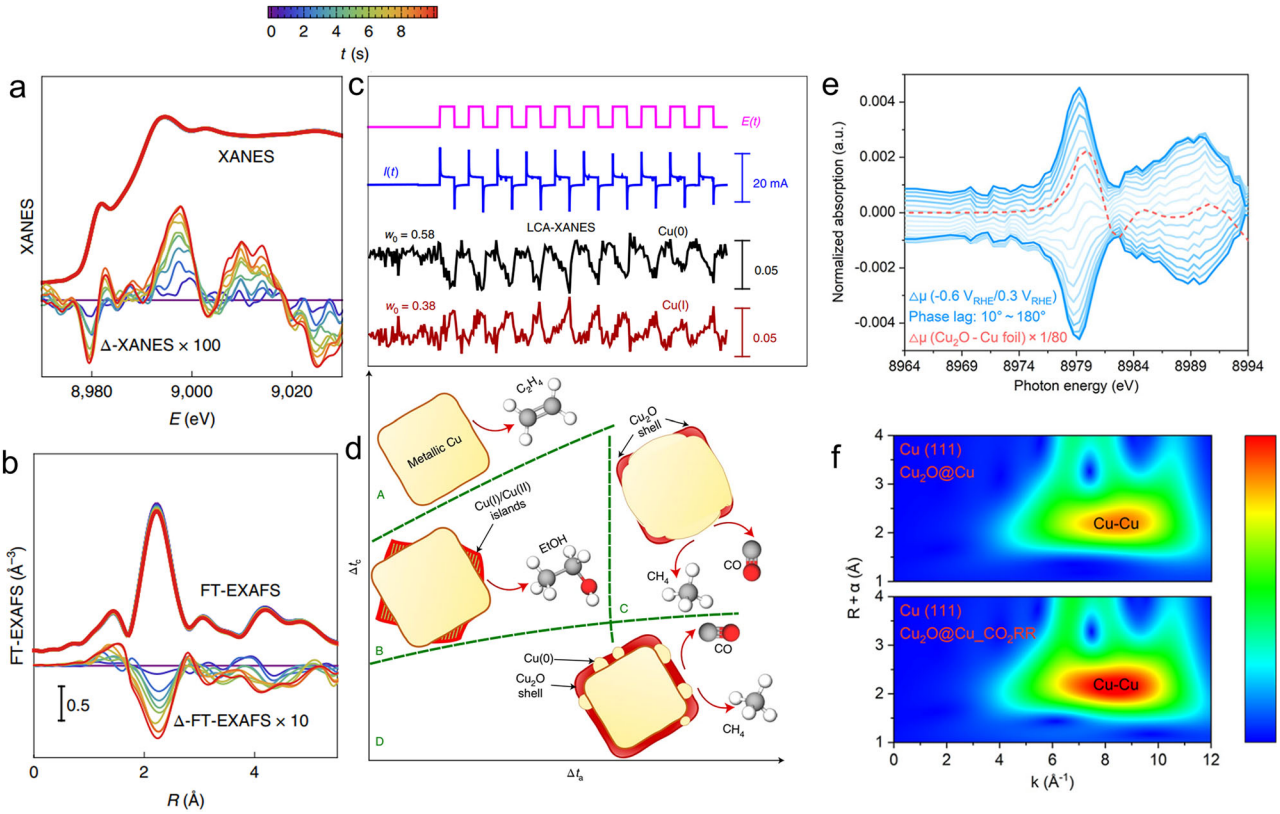

Fig. 9 | Δμ-XAFS exploring subtle changes and DAFS probing long-range and short-range structure. a, **b** Evolution of the *operando* Cu K-edge XAS under pulsed CO_2RR. Changes in XANES (**a**), EXAFS (**b**). Panels **a** and **b** show raw spectra and the differential data, where the XANES or the magnitude of the FT-EXAFS corresponding to the onset of the anodic pulse ($t = 0$) were subtracted. **c** Time dependencies of the concentrations of Cu (0) and Cu (I) species from XANES analysis. **d** Time dependencies of the concentrations of Cu (0) and Cu (I) species[76] (**a**–**d** reproduced with permission from ref. 76. Copyright 2022, Spring Nature). **e** Demodulated in situ differential spectra for phase lag between 10° and 180°. **f** Ex situ Cu (111) WT-EXAFS spectra extracted from DAFS[80] (**e**, **f** reproduced with permission from ref. 80. Copyright 2024, The Royal Society of Chemistry).

of the in-situ cell must be precisely controlled, including electrolytic cell thickness to minimize X-ray absorption, electrode positioning to prevent bubble accumulation, and window dimensions to achieve optimal balance between transmission efficiency and structural integrity. Furthermore, expanding their application to real devices for effectively analyzing operational mechanisms and deactivation processes[88]. Moreover, future efforts should concentrate on developing simplified preparation methods that leverage advanced characterization techniques. These efforts will deepen our understanding of reaction mechanisms, enhance catalyst stability and lifespan, and reduce overall costs. Ultimately, integrating this technology into industrial electrolyzers will enable meeting large-scale production demands and facilitate practical applications.

(3) Artificial intelligence (AI) assist. With the progress of 4th new generation light sources, the real-time processing of vast amounts of data will present a significant challenge. Additionally, the selection of multiple configurations of active sites and adsorption intermediates in the CO_2RR is inherently complex. AI, specifically machine learning or neural networks, offers substantial advantages in managing extensive data sets and establishing meaningful connections between theoretical model predictions and spectral features[89]. For example, Lamberti et al. utilized machine learning techniques to quantitatively fit XANES spectra to predict the geometry of Ni^{2+} surface sites adsorbed by CO_2 molecules in CPO-27–Ni[90]. Similarly, Cuenya et al. employed time-resolved *operando* XAS in combination with supervised machine learning methods to explore the local atomic and electronic structure of metallic Co sites in Co–N–C catalysts[91]. By unraveling the contributions from various co-existing species during actual reactions and deciphering their respective XAS spectra, a pathway towards understanding the CO_2RR mechanism in Co–N–C catalysts is illuminated. It is anticipated that AI-assisted XAS will revolutionize our comprehension of the CO_2RR process.

(4) Advanced characterization and synchrotron radiation multi-techniques (SRMS). The advancement of synchrotron radiation characterization technology holds a crucial position in enhancing the understanding of the micro-fine structure of catalysts. Recently, Saw Wai Hla and colleagues achieved a breakthrough by observing fingerprint spectra for individual Fe and Tb atoms through the development of a synchrotron radiation-based X-ray scanning tunneling microscope (SX-STM)[92]. Aidukas and team employed synchrotron X-ray and ptychography techniques to characterize the internal structure of microchips, achieving an unprecedented resolution of 4 nm images[93]. Considering that the CO_2RR involves changes in various parameters such as phase structure, electronic state, local geometry, reaction absorption, and desorption, the use of SRMS allows for in-situ multi-dimensional monitoring of catalysts. Techniques like gas chromatography–mass spectrometry (GC–MS), IR, Raman spectroscopy, UV–vis spectroscopy, and XAS can be combined to investigate complex system dynamics. Additionally, the integration of XAFS with XRD enables the examination of both short-range and long-range ordered structures[94]. Undoubtedly, this coupling technique involving multiple light beams at the same sample location while conducting different experiments simultaneously serves as an effective approach to explore solid–liquid–gas three-phase interfaces[95–97].

(5) Considerations for a thorough understanding of high-flux X-ray photon beams in electrochemistry field. One less discussed hurdle for investigating electrochemical processes with high flux X-ray photon beams is the undesirable beam damage. Fundamentally, beam damage manifests as a radiolysis phenomenon, where molecular bonds break upon exposure to high-energy radiation. During in-situ reactions, incoming gas molecules undergo photoelectric effects and inelastic scattering through interaction with high-energy X-rays. This interaction leads to gas ionization and excitation, generating chemically reactive free radicals and active species that trigger sample decomposition and induce surface chemical reactions. Several protective strategies against beam-induced damage have proven effective. These include utilizing lower incident flux beamlines generated by bending magnet devices, implementing rapid scanning modes to reduce exposure time, employing continuous flow systems for sample renewal, and selecting radiation-resistant materials for sample chambers. Parasitic currents present another significant challenge, arising from multiple sources that impact electrochemical performance. These currents originate from X-ray ionization-induced photogenerated carriers, photoelectric effects at sample and electrode interfaces, and conductive species formed through solution radiolysis. Ensuring measurement accuracy requires careful control of experimental conditions through strategic approaches, including appropriate background correction methods and judicious selection of reference electrodes. Of equal importance is the management of bubble formation, which occurs through both solvent radiolysis and electrochemical reaction products. This challenge necessitates optimized in-situ electrolysis cell design to minimize bubble accumulation. Additionally, real-time monitoring of evolved gases via GC-MS enables continuous analysis of reaction products, allowing researchers to refine experimental parameters dynamically and ensure accurate observation of authentic reaction processes.

Received: 18 November 2024; Accepted: 12 March 2025;
Published online: 04 April 2025

References

1. Obama, B. The irreversible momentum of clean energy. *Science* **355**, 126–129 (2017).
2. De Luna, P. et al. What would it take for renewably powered electrosynthesis to displace petrochemical processes? *Science* **364**, eaav3506 (2019).
3. Gao, W. et al. Industrial carbon dioxide capture and utilization: state of the art and future challenges. *Chem. Soc. Rev.* **49**, 8584–8686 (2020).
4. Chu, S. & Majumdar, A. Opportunities and challenges for a sustainable energy future. *Nature* **488**, 294–303 (2012).
5. Artz, J. et al. Sustainable conversion of carbon dioxide: an integrated review of catalysis and life cycle assessment. *Chem. Rev.* **118**, 434–504 (2018).
6. Yang, Y. et al. Operando studies reveal active Cu nanograins for CO_2 electroreduction. *Nature* **614**, 262–269 (2023).
7. Nitopi, S. et al. Progress and perspectives of electrochemical CO_2 reduction on copper in aqueous electrolyte. *Chem. Rev.* **119**, 7610–7672 (2019).
8. Kim, J. Y. T., Sellers, C., Hao, S., Senftle, T. P. & Wang, H. Different distributions of multi-carbon products in CO_2 and CO electroreduction under practical reaction conditions. *Nat. Catal.* **6**, 1115–1124 (2023).
9. Sharifian, R., Wagterveld, R. M., Digdaya, I. A., Xiang, C. & Vermaas, D. A. Electrochemical carbon dioxide capture to close the carbon cycle. *Energy Environ. Sci.* **14**, 781–814 (2021).
10. Gattrell, M., Gupta, N. & Co, A. A review of the aqueous electrochemical reduction of CO_2 to hydrocarbons at copper. *J. Electroanal. Chem.* **594**, 1–19 (2006).
11. Wang, J., Tan, H. Y., Zhu, Y., Chu, H. & Chen, H. M. Linking the dynamic chemical state of catalysts with the product profile of electrocatalytic CO_2 reduction. *Angew. Chem. Int. Ed.* **60**, 17254–17267 (2021).
12. Lai, W. et al. Dynamic evolution of active sites in electrocatalytic CO_2 reduction reaction: fundamental understanding and recent progress. *Adv. Funct. Mater.* **32**, 2111193 (2022).
13. Gu, H. et al. A two-dimensional van der Waals heterostructure with isolated electron-deficient cobalt sites toward high-efficiency CO_2 electroreduction. *J. Am. Chem. Soc.* **144**, 21502–21511 (2022).
14. Jeon, H. S. et al. Operando insight into the correlation between the structure and composition of CuZn nanoparticles and their selectivity for the electrochemical CO_2 reduction. *J. Am. Chem. Soc.* **141**, 19879–19887 (2019).
15. Cao, X. et al. In situ characterization for boosting electrocatalytic carbon dioxide reduction. *Small Methods* **5**, 2100700 (2021).
16. Handoko, A. D., Wei, F., Jenndy, Yeo, B. S. & Seh, Z. W. Understanding heterogeneous electrocatalytic carbon dioxide reduction through operando techniques. *Nat. Catal.* **1**, 922–934 (2018).
17. Deng, Y. & Yeo, B. S. Characterization of electrocatalytic water splitting and CO_2 reduction reactions using in situ/operando raman spectroscopy. *ACS Catal.* **7**, 7873–7889 (2017).
18. Zeng, Z. C. et al. Electrochemical tip-enhanced raman spectroscopy. *J. Am. Chem. Soc.* **137**, 11928–11931 (2015).
19. Chen, L. X. & Yano, J. Deciphering photoinduced catalytic reaction mechanisms in natural and artificial photosynthetic systems on multiple temporal and spatial scales using X-ray probes. *Chem. Rev.* **124**, 5421–5469 (2024).
20. Zhu, Y. et al. Emerging dynamic structure of electrocatalysts unveiled by in situ X-ray diffraction/absorption spectroscopy. *Energy Environ. Sci.* **14**, 1928–1958 (2021).
21. Xu, Y. N. et al. In situ/operando synchrotron radiation analytical techniques for CO_2/CO reduction reaction: from atomic scales to mesoscales. *Angew. Chem. Int. Ed.* **63**, e202404213 (2024).
22. Huang, H. & Russell, A. E. Approaches to achieve surface sensitivity in the in situ XAS of electrocatalysts. *Curr. Opin. Electrochem* **27**, 100681 (2021).
23. Ren, B. et al. Nano-crumples induced Sn-Bi bimetallic interface pattern with moderate electron bank for highly efficient CO_2 electroreduction. *Nat. Commun.* **13**, 2486 (2022).
24. Sun, Z., Liu, Q., Yao, T., Yan, W. & Wei, S. X-ray absorption fine structure spectroscopy in nanomaterials. *Sci. China Mater.* **58**, 313–341 (2015).
25. Wang, B. et al. Application of X-ray absorption spectroscopy in electrocatalytic water splitting and CO_2 reduction. *Small Sci.* **1**, 2100023 (2021).
26. Tian, X. et al. Engineering bunched Pt-Ni alloy nanocages for efficient oxygen reduction in practical fuel cells. *Science* **366**, 850–856 (2019).
27. Li, J. & Gong, J. Operando characterization techniques for electrocatalysis. *Energy Environ. Sci.* **13**, 3748–3779 (2020).
28. Timoshenko, J. & Roldan Cuenya, B. In situ/operando electrocatalyst characterization by X-ray absorption spectroscopy. *Chem. Rev.* **121**, 882–961 (2021).
29. Yang, Y. et al. Operando methods in electrocatalysis. *ACS Catal.* **11**, 1136–1178 (2021).
30. Lin, S. C. et al. Operando time-resolved X-ray absorption spectroscopy reveals the chemical nature enabling highly selective CO_2 reduction. *Nat. Commun.* **11**, 3525 (2020).
31. Feijóo, J. et al. Operando high-energy-resolution X-ray spectroscopy of evolving Cu nanoparticle electrocatalysts for CO_2 reduction. *J. Am. Chem. Soc.* **145**, 20208–20213 (2023).
32. Yun, H., Choi, W., Shin, D., Oh, H. S. & Hwang, Y. J. Atomic arrangement of auag alloy on carbon support enhances

electrochemical CO_2 reduction in membrane electrode assembly. *ACS Catal.* **13**, 9302–9312 (2023).
33. de Ruiter, J. et al. Probing the dynamics of low-overpotential CO_2-to-CO activation on copper electrodes with time-resolved raman spectroscopy. *J. Am. Chem. Soc.* **144**, 15047–15058 (2022).
34. Gauthier, J. A. et al. Facile electron transfer to CO_2 during adsorption at the metal|solution interface. *J. Phys. Chem. C* **123**, 29278–29283 (2019).
35. Wang, G. et al. Electrocatalysis for CO_2 conversion: from fundamentals to value-added products. *Chem. Soc. Rev.* **50**, 4993–5061 (2021).
36. Nam, D.-H. et al. Molecular enhancement of heterogeneous CO_2 reduction. *Nat. Mater.* **19**, 266–276 (2020).
37. Iglesias-Juez, A., Chiarello, G. L., Patience, G. S. & Guerrero-Pérez, M. O. Experimental methods in chemical engineering: X-ray absorption spectroscopy-XAS, XANES, EXAFS. *Can. J. Chem. Eng.* **100**, 3–22 (2022).
38. Yang, H. B. et al. Atomically dispersed Ni(I) as the active site for electrochemical CO_2 reduction. *Nat. Energy* **3**, 140–147 (2018).
39. Han, M. H. et al. Real-time mimicking the electronic structure of N-coordinated Ni single atoms: NiS-enabled electrochemical reduction of CO_2 to CO. *Adv. Energy Mater.* **12**, 2201843 (2022).
40. Okatenko, V. et al. Alloying as a strategy to boost the stability of copper nanocatalysts during the electrochemical CO_2 reduction reaction. *J. Am. Chem. Soc.* **145**, 5370–5383 (2023).
41. Shen, X. et al. Synergistic modulation at atomically dispersed Fe/Au interface for selective CO_2 electroreduction. *Nano Lett.* **21**, 686–692 (2021).
42. Wang, Z. et al. Identification of synergies in Fe, Co-coordinated polyphthalocyanines scaffolds for electrochemical CO_2 reduction reaction. *Nano Lett.* **24**, 3249–3256 (2024).
43. Zhang, X. Y. et al. In operando identification of in situ formed metalloid zincδ+ active sites for highly efficient electrocatalyzed carbon dioxide reduction. *Angew. Chem. Int. Ed.* **61**, e202202298 (2022).
44. Ko, Y. J. et al. Extrinsic hydrophobicity-controlled silver nanoparticles as efficient and stable catalysts for CO_2 electrolysis. *Nat. Commun.* **15**, 3356 (2024).
45. Ko, Y. J. et al. Exploring dopant effects in stannic oxide nanoparticles for CO_2 electro-reduction to formate. *Nat. Commun.* **13**, 2205 (2022).
46. Zhang, B. et al. Steering CO_2 electroreduction toward methane or ethylene production. *Nano Energy* **88**, 106239 (2021).
47. Zhang, X. Y. et al. Direct OC-CHO coupling towards highly C_{2+} products selective electroreduction over stable Cu^0/Cu^{2+} interface. *Nat. Commun.* **14**, 7681 (2023).
48. Wang, Y. et al. Precisely constructing orbital coupling-modulated dual-atom Fe pair sites for synergistic CO_2 electroreduction. *ACS Energy Lett.* **7**, 640–649 (2022).
49. Zeng, Y. et al. Unraveling the electronic structure and dynamics of the atomically dispersed iron sites in electrochemical CO_2 reduction. *J. Am. Chem. Soc.* **145**, 15600–15610 (2023).
50. Liu, X. et al. Dynamic surface reconstruction of single-atom bimetallic alloy under operando electrochemical conditions. *Nano Lett.* **20**, 8319–8325 (2020).
51. Martini, A. et al. Tracking the evolution of single-atom catalysts for the CO_2 electrocatalytic reduction using operando X-ray absorption spectroscopy and machine learning. *J. Am. Chem. Soc.* **145**, 17351–17366 (2023). **Combination of unsupervised and supervised machine learning approaches to decipher the XANES of the TMNCs, disentangling the contributions of different metal sites coexisting in the working catalyst**.
52. Funke, H., Chukalina, M. & Rossberg, A. Wavelet analysis of extended X-ray absorption fine structure data. *Phys. Scr.* **2005**, 232 (2005).
53. Funke, H., Chukalina, M. & Scheinost, A. C. A new FEFF-based wavelet for EXAFS data analysis. *J. Synchrotron Radiat.* **14**, 426–432 (2007).
54. Xia, Z., Zhang, H., Shen, K., Qu, Y. & Jiang, Z. Wavelet analysis of extended X-ray absorption fine structure data: theory, application. *Physica B* **542**, 12–19 (2018).
55. He, Q. et al. Electrochemical conversion of CO_2 to syngas with controllable CO/H_2 ratios over Co and Ni single-atom catalysts. *Angew. Chem. Int. Ed.* **59**, 3033–3037 (2020).
56. Xiong, W. F. et al. Steering CO_2 electroreduction selectivity U-turn to ethylene by Cu-Si bonded interface. *J. Am. Chem. Soc.* **146**, 289–297 (2024).
57. Li, J. et al. Selective CO_2 electrolysis to CO using isolated antimony alloyed copper. *Nat. Commun.* **14**, 340 (2023).
58. Zhou, Y. et al. Asymmetric dinitrogen-coordinated nickel single-atomic sites for efficient CO_2 electroreduction. *Nat. Commun.* **14**, 3776 (2023).
59. Cao, D., Shou, H., Chen, S. & Song, L. Manipulating and probing the structural self-optimization in oxygen evolution reaction catalysts. *Curr. Opin. Electrochem* **30**, 100788 (2021).
60. Hsu, C. S. et al. Activating dynamic atomic-configuration for single-site electrocatalyst in electrochemical CO_2 reduction. *Nat. Commun.* **14**, 5245 (2023).
61. Huang, J. E. et al. CO_2 electrolysis to multicarbon products in strong acid. *Science* **372**, 1074–1078 (2021).
62. Sheng, B. et al. Anomalous Ru dissolution enabling efficient integrated CO_2 electroreduction in strong acid. *Chem. Eng. J.* **454**, 140245 (2023).
63. Fang, W. et al. Durable CO_2 conversion in the proton-exchange membrane system. *Nature* **626**, 86–91 (2024).
64. Frahm, R. Quick scanning exafs: First experiments. *Nucl. Instrum. Methods Phys. Res. Sect. A* **270**, 578–581 (1988).
65. Rüscher, M. et al. Tracking heterogeneous structural motifs and the redox behaviour of copper-zinc nanocatalysts for the electrocatalytic CO_2 reduction using operando time resolved spectroscopy and machine learning. *Catal. Sci. Technol.* **12**, 3028–3043 (2022).
66. Niu, W. et al. Pb-rich Cu grain boundary sites for selective CO-to-n-propanol electroconversion. *Nat. Commun.* **14**, 4882 (2023).
67. Herzog, A. et al. Time-resolved operando insights into the tunable selectivity of Cu-Zn nanocubes during pulsed CO_2 electroreduction. *Energy Environ. Sci.* **17**, 7081–7096 (2024).
68. Timoshenko, J. et al. Reversible metal cluster formation on Nitrogen-doped carbon controlling electrocatalyst particle size with subnanometer accuracy. *Nat. Commun.* **15**, 6111 (2024). **Using operando quick X-ray absorption spectroscopy tracking the catalyst's evolution: fragmentation of the Cu particles and partial regeneration of single atom sites**.
69. Hämäläinen, K., Siddons, D. P., Hastings, J. B. & Berman, L. E. Elimination of the inner-shell lifetime broadening in X-ray-absorption spectroscopy. *Phys. Rev. Lett.* **67**, 2850–2853 (1991).
70. Krause, M. O. & Oliver, J. H. Natural widths of atomic K and L levels, Kα X-ray lines and several KLL Auger lines. *J. Phys. Chem. Ref. Data* **8**, 329–338 (1979).
71. Rovezzi, M. & Glatzel, P. Hard X-ray emission spectroscopy: a powerful tool for the characterization of magnetic semiconductors. *Semicond. Sci. Technol.* **29**, 023002 (2014).
72. Sokaras, D. et al. A seven-crystal Johann-type hard X-ray spectrometer at the Stanford Synchrotron Radiation Lightsource. *Rev. Sci. Instrum.* **84**, 053102 (2013).
73. Wang, J. et al. In situ X-ray spectroscopies beyond conventional X-ray absorption spectroscopy on deciphering dynamic configuration of electrocatalysts. *Nat. Commun.* **14**, 6576 (2023). **Introducing advanced X-ray spectroscopies beyond conventional XAS, with**

emphasis on their unprecedented capabilities of deciphering key configurations of electrocatalysts.
74. Chen, P.-C. et al. Chemical and structural evolution of AgCu catalysts in electrochemical CO_2 reduction. *J. Am. Chem. Soc.* **145**, 10116–10125 (2023).
75. Mei, B. et al. Operando HERFD-XANES and surface sensitive Δμ analyses identify the structural evolution of copper(II) phthalocyanine for electroreduction of CO_2. *J. Energy Chem.* **64**, 1–7 (2022).
76. Timoshenko, J. et al. Steering the structure and selectivity of CO_2 electroreduction catalysts by potential pulses. *Nat. Catal.* **5**, 259–267 (2022). **Employing operando X-ray absorption and X-ray diffraction methods with sub-second time resolution to unveil the surprising complexity of catalysts exposed to dynamic reaction conditions**.
77. Cross, J. O., Elam, W. T., Woicik, J. & Sorensen, L. B. Reliability of structural parameters determined from DAFS data using the iterative dispersion integral algorithm. *J. Synchrotron Radiat.* **6**, 335–337 (1999).
78. Pickering, I. J., Sansone, M., Marsch, J. & George, G. N. Diffraction anomalous fine structure: a new technique for probing local atomic environment. *J. Am. Chem. Soc.* **115**, 6302–6311 (1993).
79. Stragier, H. et al. Diffraction anomalous fine structure: a new x-ray structural technique. *Phys. Rev. Lett.* **69**, 3064–3067 (1992).
80. Qiao, S. et al. Stepped copper sites coupling voltage-induced surfactant assembly to achieve efficient CO_2 electroreduction to formate. *Energy Environ. Sci.* **17**, 6779–6786 (2024). **Employing electrochemical modulating XAFS and DAFS spectra elucidated the transformation from the heterostructure of Cu2O and Cu to stepped Cu sites**.
81. Cheng, Y., Hou, J. & Kang, P. Integrated capture and electroreduction of flue gas CO_2 to formate using amine functionalized SnO_x nanoparticles. *ACS Energy Lett.* **6**, 3352–3358 (2021).
82. Huang, Y. et al. Preorganization and cooperation for highly efficient and reversible capture of low-concentration CO_2 by ionic liquids. *Angew. Chem. Int. Ed.* **56**, 13293–13297 (2017).
83. Zhao, Z.-H. et al. Efficient capture and electroreduction of dilute CO_2 into highly pure and concentrated formic acid aqueous solution. *J. Am. Chem. Soc.* **146**, 14349–14356 (2024).
84. Kim, D. et al. Electrocatalytic reduction of low concentrations of CO_2 gas in a membrane electrode assembly electrolyzer. *ACS Energy Lett.* **6**, 3488–3495 (2021).
85. Jouny, M. et al. Formation of carbon-nitrogen bonds in carbon monoxide electrolysis. *Nat. Chem.* **11**, 846–851 (2019).
86. Zhu, X., Zhou, X., Jing, Y. & Li, Y. Electrochemical synthesis of urea on MBenes. *Nat. Commun.* **12**, 4080 (2021).
87. Wang, X. et al. Mechanistic reaction pathways of enhanced ethylene yields during electroreduction of CO_2-CO co-feeds on Cu and Cu-tandem electrocatalysts. *Nat. Nanotechnol.* **14**, 1063–1070 (2019).
88. Sheng, B. et al. Application of X-ray absorption spectroscopy in carbon-supported electrocatalysts. *Nano Res.* **16**, 12438–12452 (2023).
89. Zhong, M. et al. Accelerated discovery of CO_2 electrocatalysts using active machine learning. *Nature* **581**, 178–183 (2020).
90. Guda, A. A. et al. Machine learning approaches to XANES spectra for quantitative 3D structural determination: the case of CO_2 adsorption on CPO-27-Ni MOF. *Radiat. Phys. Chem.* **175**, 108430 (2020).
91. Martini, A. et al. Revealing the structure of the active sites for the electrocatalytic CO_2 reduction to CO over Co single atom catalysts using operando XANES and machine learning. *J. Synchrotron Radiat.* **31**, 741–750 (2024).
92. Ajayi, T. M. et al. Characterization of just one atom using synchrotron X-rays. *Nature* **618**, 69–73 (2023).
93. Gorkhover, T. & Rupp, D. Microchip minutiae imaged using rapid X-ray bursts. *Nature* **632**, 36–38 (2024).
94. Sekizawa, O. et al. Simultaneous operando time-resolved XAFS-XRD measurements of a Pt/C cathode catalyst in polymer electrolyte fuel cell under transient potential operations. *ACS Sustain. Chem. Eng.* **5**, 3631–3636 (2017).
95. Sheng, B., Cao, D., Liu, C., Chen, S. & Song, L. Support effects in electrocatalysis and their synchrotron radiation-based characterizations. *J. Phys. Chem. Lett.* **12**, 11543–11554 (2021).
96. He, Q. et al. Phase engineering and synchrotron-based study on two-dimensional energy nanomaterials. *Chem. Rev.* **123**, 10750–10807 (2023).
97. Cao, D. et al. Visualizing catalytic dynamics processes via synchrotron radiation multitechniques. *Adv. Mater.* **35**, 2205346 (2023).
98. Xu, W. et al. Approach to electrochemical modulating differential extended X-ray absorption fine structure. *J. Synchrotron Radiat.* **29**, 1065–1073 (2022).

Acknowledgements

This work was financially supported in part by National Key R&D Program of China (2022YFA1605400), NSFC (12225508, 12322515, U23A20121, 22075264, 12205303 and 12305370), CAS Youth Innovation Promotion Association (2022457) and the Strategic Priority Research Program (XDA0410401), China Postdoctoral Science Foundation (BX20220282 and 2022M720136), Anhui Provincial Natural Science Foundation (2308085Q A16) and the Fundamental Research Funds for the Central Universities (WK2060000099). We thank the Shanghai Synchrotron Radiation Facility (BL14W1, BL02B02, SSRF), Beijing Synchrotron Radiation Facility (1W1B, 4B7A, BSRF), the Hefei Synchrotron Radiation Facility (Infrared Spectros copy and Microspectroscopy, MCD-A and MCD-B Soochow Beamline for Energy Materials at NSRL), the USTC Instruments Center for Physical Science as well as Center for Micro and Nanoscale Research and Fabrication for helps.

Author contributions

S.L., W.J., and C.S. conceptualized and supervised the review; S.B. prepared the initial and revised paper; C.D. and Z.N. revised the paper; S.L., C.S., and C.D. acquired funding for this work.

Competing interests

The authors declare no competing interests.

Additional information

Supplementary information The online version contains supplementary material available at https://doi.org/10.1038/s43246-025-00779-2.

Correspondence and requests for materials should be addressed to Shuangming Chen, Jianqiang Wang or Li Song.

Peer review information *Communications Materials* thanks the anonymous reviewers for their contribution to the peer review of this work. Primary Handling Editors: Haotian Wang and Jet-Sing Lee. A peer review file is available.